nature structural & molecular biology

Min protein patterns emerge from rapid rebinding and membrane interaction of MinE

Martin Loose[1,2], Elisabeth Fischer-Friedrich[3], Christoph Herold[1], Karsten Kruse[4] & Petra Schwille[1,2]

In *Escherichia coli*, the pole-to-pole oscillation of the Min proteins directs septum formation to midcell, which is required for symmetric cell division. *In vitro*, protein waves emerge from the self-organization of MinD, a membrane-binding ATPase, and its activator MinE. For wave propagation, the proteins need to cycle through states of collective membrane binding and unbinding. Although MinD presumably undergoes cooperative membrane attachment, it is unclear how synchronous detachment is coordinated. We used confocal and single-molecule microscopy to elucidate the order of events during Min wave propagation. We propose that protein detachment at the rear of the wave, and the formation of the E-ring, are accomplished by two complementary processes: first, local accumulation of MinE due to rapid rebinding, leading to dynamic instability; and second, a structural change induced by membrane-interaction of MinE in an equimolar MinD–MinE (MinDE) complex, which supports the robustness of pattern formation.

Before cells divide, they need to define the site of cell division. In the bacterium *E. coli*, the precise placement of cytokinesis primarily depends on the Min system. The Min system is composed of the proteins MinC, MinD and MinE, which oscillate between the two poles of the cell[1–6], ensuring that polymerization of FtsZ, the initial event of cell division, only occurs at the middle of the cell.

The oscillation is driven by the ATPase MinD and its activator MinE[7]. MinC, which binds to membrane-bound MinD, is not required for the oscillation[2,3,5,8] but is the actual inhibitor of FtsZ polymerization[9,10]. MinE and MinC bind to overlapping sites on MinD. *In vitro* co-sedimentation assays have shown that MinE is able to displace MinC from membrane-bound MinD before it stimulates ATP hydrolysis by MinD and detachment of the proteins from the membrane[11,12].

During one oscillation cycle, a complex of MinD and MinC homogenously covers the membrane of roughly one cell. In this polar cap, both proteins start to detach from close to midcell and then rebind in the opposite half. Although MinE is also seen on the entire MinD cap, the highest portion of this protein can be found at the rim of the shrinking polar MinCD cap in a prominent ring close to midcell, the so-called E-ring[6]. Consistent with the observation of the E-ring *in vivo*, the maximum density of MinE can be found at the rear of the wave *in vitro*, located behind the maximum density of MinD, where it delimits the propagating protein band[13].

Biochemical oscillations only occur in nonlinear dynamical systems[14,15]. One source of nonlinearity required for the dynamic instability and oscillation of the Min system may be the initial cooperative binding of MinD to the membrane. This cooperativity is probably due, at least in part, to membrane-dependent dimerization of MinD[11,16,17]. The sharp decrease in protein densities at the end of the oscillation cycle also argues for collective effects during protein detachment from the membrane. Collective detachment of proteins is thought to be initiated by the E-ring, but how MinE can accumulate to form this ring at the rim of the shrinking MinCD zone is not well understood. Theoretical modeling of the Min oscillations has suggested that either cooperative binding of MinE[13,18] or augmented binding of MinE to the rim of the MinD cap because of a high binding rate and slow cytoplasmic diffusion[19] of MinE can give rise to the E-ring. Other theoretical models have suggested that the E-ring is generated by persistent binding of MinE to the MinD cap, either because of rapid rebinding[20,21] or because of transient interaction with the membrane of MinE[22]. It has also been proposed that the E-ring represents dimerized MinE, whereas monomeric MinE would be present outside of the ring[6,17]. One reason for the large variety of mechanisms suggested for E-ring formation is that information about the spatiotemporal dynamics of Min proteins during pattern formation is difficult to obtain from bulk biochemical assays. Furthermore, simultaneous imaging of all three Min proteins *in vivo* and *in vitro* has not yet been achieved.

To better understand the mechanism by which the E-ring forms and to elucidate its role for Min protein pattern formation, we experimentally studied the order of events during propagation of waves of all three Min proteins, MinD, MinE and MinC *in vitro*. Our data show that MinE accumulates toward the rear of the traveling wave by rapid rebinding to the membrane-bound layer of MinD, and not by cooperative binding or dimerization of MinE. As a result of MinE rebinding, every MinD dimer located at the rear of the wave is present in an equimolar complex with its activator MinE. Furthermore, we found

[1]Biophysics, BIOTEC, Dresden University of Technology, Dresden, Germany. [2]Max Planck Institute for Molecular Cell Biology and Genetics, Dresden, Germany. [3]Max Planck Institute for the Physics of Complex Systems, Dresden, Germany. [4]Theoretische Physik, Universitaet des Saarlandes, Saarbruecken, Germany. Correspondence should be addressed to P.S. (petra.schwille@biotec.tu-dresden.de).

Received 28 July 2010; accepted 11 February 2011; published online 24 April 2011; doi:10.1038/nsmb.2037

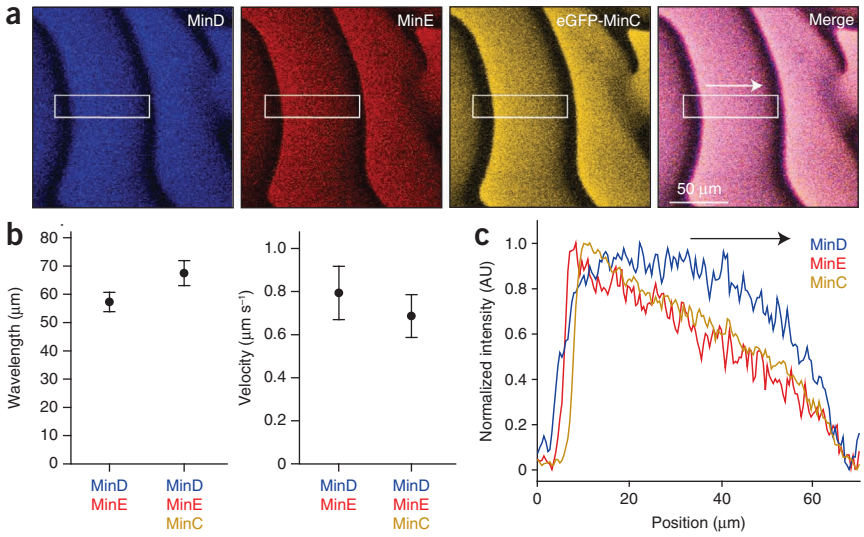

Figure 1 MinD, MinE and eGFP-MinC in traveling waves *in vitro*. (**a**) Confocal fluorescence micrographs showing waves of MinD (0.8 μM with 10 mol % MinD-Cy3), MinE (1.2 μM MinE with 10 mol % MinE-Cy5) and MinC (0.08 μM, with 40 mol % His-eGFP–MinC) on a supported lipid membrane. (**b**) The influence of the presence of MinC on velocity and period of the protein waves. Error bars represent s.d., $n = 9$. (**c**) Fluorescence intensity profiles of MinD, MinE and MinC acquired from the rectangular region shown in **a**. Starting from the front of the wave (right), the density of MinC rises at a slope similar to that of MinE and also shows a similar sharp decrease at the rear of the wave. Note that the detachment of MinC is shifted toward the front of the wave.

evidence that in this complex, the interaction of MinE with the membrane is required in order to exclude MinC from the membrane-bound protein layer. We propose that these two processes are crucial for the acceleration of protein detachment at the rear of the wave, or at the end of an oscillation cycle, to efficiently clear the membrane of proteins.

RESULTS

In vitro reconstitution of MinCDE waves

MinE has been found to be able to displace MinC from the MinCD complex in a step that is independent of ATP hydrolysis[11,12], demonstrating that MinE first successfully competes for the binding site on MinD and then stimulates MinD detachment. However, without simultaneous imaging of all three Min proteins, the spatial and temporal order of these events during pattern formation has remained unclear. To address these limitations, we incubated purified MinD (0.8 μM, with 10 mol % MinD labeled with Cy5) and MinE (1.2 μM, with 10 mol % MinE labeled with Cy3), together with MinC (0.08 μM, with 40 mol % of an eGFP–MinC fusion protein) in the presence of ATP on a supported lipid bilayer[13]. This concentration ratio corresponds to the one found *in vivo*[23,24]. When incorporated into traveling Min-protein waves, MinC did not change the intensity profiles of MinE and MinD (**Fig. 1a** and **Supplementary Video 1**) and only led to a slightly larger period (68.1 ± 5.9 μm compared to 58.4 ± 9.9 μm; mean ± s.d., $n = 9$, $P = 0.0225$) and decreased velocity (0.69 ± 0.10 μm s^{-1} compared to 0.79 ± 0.12 μm s^{-1}; mean ± s.d., $n = 9$, $P = 0.0728$) of the wave (**Fig. 1b**). The intensity profile of MinC within the protein band resembles that of MinE (**Fig. 1c**). After a transitory phase at the wave front, the MinC density increases linearly and then drops in a manner that is similar to MinE. However, compared to the MinE distribution, the sudden collapse of MinC density occurs 2–3 μm before membrane detachment of MinE from the membrane (2.55 ± 0.80 μm, mean ± s.d., $n = 5$). Because the pattern *in vitro* is about ten times larger than *in vivo*[13], this value corresponds to a width of 0.2–0.3 μm in the *E. coli* cell. Our findings suggest that MinE does not inhibit initial binding of MinC to MinD, but that MinE forms a tight complex with MinD at the rear of the wave, causing collective MinC displacement from the membrane-bound MinD layer.

Accumulation of MinE precedes detachment of MinD and MinC

Using confocal microscopy, we could not observe a unique MinE structure at the rear of the protein wave, which could explain how MinE can trigger simultaneous MinC detachment. To reduce the background fluorescence from proteins not binding to the membrane, we used total internal reflection fluorescence (TIRF) microscopy, where the excitation light is restricted to a narrow region above the membrane. In TIRF micrographs, a narrow, bright band of MinE is readily observable at the trailing edge of the wave (**Fig. 2** and **Supplementary Video 2**). This band of high intensity is also visible in corresponding kymographs (**Fig. 2b**,**f**). Starting from the wave front, the density of MinE increases linearly, and then peaks at the rear, before it suddenly collapses (red line in **Fig. 2c**,**g**). The signal of MinD increases faster than MinE and nonlinearly (see blue line in **Fig. 2c**).

By comparing the fluorescence intensities of the membrane-bound proteins to calibration standards, we could estimate the density of membrane-bound proteins[25]. We found that the peak protein-surface density of MinD was 1.62×10^4 μm^{-2} ± 27.2% (s.e.m., $n = 4$), which was two times higher than the peak density of MinE (0.73×10^4 μm^{-2} ± 7.6%; s.e.m., $n = 4$; see **Supplementary Fig. 1** and **Supplementary Methods**). Using these values to rescale the fluorescence intensity profiles of MinD and MinE, we could calculate the ratio of the protein densities [MinE]/[MinD] within the protein band. We found that this ratio continuously rises and peaks at the rear of the wave at a value of about 0.9 (0.87 ± 0.17, s.e.m., $n = 4$; see black curve in **Fig. 2d** inset), suggesting that at the maximum density of MinE, nearly every MinD dimer on the membrane is in an equimolar complex with its activator MinE.

To better understand how the changes in the densities of MinE and MinD relate to each other, we calculated the derivatives of the intensity profiles (**Fig. 2d**). The derivative of the MinD profile shows that, starting from the wave front, accumulation of MinD on the membrane is initially fast, but then slows down until detachment of MinD from the membrane starts to dominate. We found it remarkable that the rate of MinD density change goes along with the change of the [MinE]/[MinD] ratio, with the highest rate of MinD detachment coinciding with the maximum [MinE]/[MinD] ratio (**Fig. 2d** inset).

A comparison of the intensity profiles of MinC and MinE reveals that synchronous detachment of MinC coincides with the maximum density increase of MinE (**Fig. 2h**), indicating that, in this case, MinD and MinE form a tight membrane-bound complex, which efficiently excludes MinC from the protein band.

To summarize, these results illustrate that protein binding and detachment within the traveling protein band is governed by the ratio of MinE to MinD on the membrane. This ratio also dictates the directionality of wave propagation, because the ratio and the MinD detachment rate have their maxima at the rear of the wave.

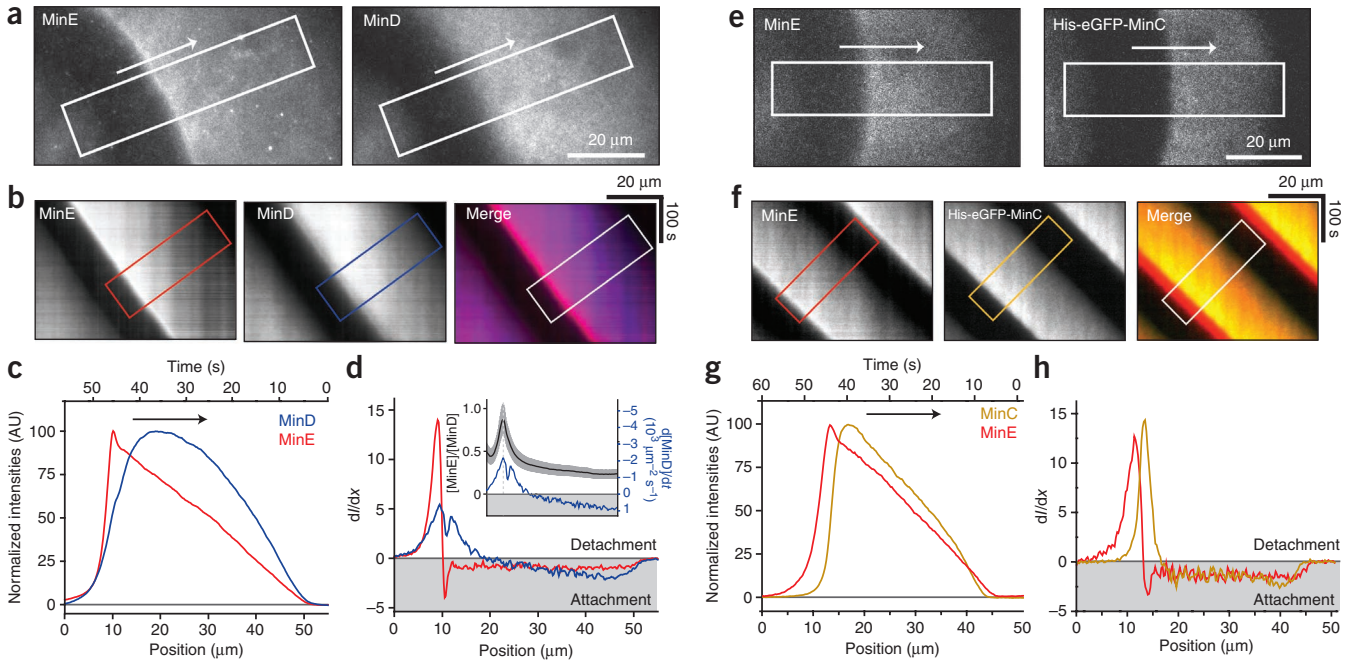

Figure 2 Dynamics of Min proteins and their relationships. (**a**) Typical TIRF microscopy micrographs of surface waves formed by MinD (0.8 μM with 5 mol % MinD–Alexa 488) and MinE (1.2 μM MinE with 5 mol % MinE-Cy5). (**b**) Kymographs associated with rectangular regions in **a**. (**c**) Normalized intensity plots obtained from the kymographs, representing averaged intensity distributions. Because the waves move at a constant speed v, the spatial profile corresponds to a temporal sequence where the spatial position x is related to time t by the relationship $x = vt$. (**d**) Derivatives of the intensity plots shown in **c**. Inset in **d**: black line is the ratio of MinE and MinD surface densities (gray region represents s.e.m, $n = 4$); blue line is the derivative of normalized MinD intensity (see **Supplementary Fig. 1**). (**e**–**h**) As in **a**–**d**, with His-eGFP-MinC (0.02 μM) instead of MinD–Alexa 488.

MinE accumulates because of wave propagation

How can the density of MinE increase toward the rear of the wave, while the density of its binding partner MinD is decreasing? It has been proposed that MinE forms the E–ring by dimerization; that is, MinE would first bind as a monomer to membrane-bound MinD and later dimerize, thereby increasing in density to give rise to the ring[6,17]. To test this possibility, we designed an experiment to measure the FRET efficiency between MinE monomers labeled with either Cy3 (donor) or Cy5 (acceptor). The fluorophores were attached to a residue located at the monomer-monomer interface in the MinE dimer (see **Supplementary Fig. 2**).

In the case of FRET, the donor fluorescence is quenched by energy transfer to the acceptor. Destroying the acceptor fluorophore by photobleaching will result in a fluorescence increase of the donor fluorophore[26]. We used MinE labeled with Cy3 and Cy5 to initiate pattern formation. After parallel surface waves had formed, we bleached a rectangular area of MinE-Cy5 (acceptor) and recorded the change in fluorescence of MinE-Cy3 (donor). As shown in **Figure 3a**,**b**, the fluorescence intensity of the donor increased after the acceptor dye was bleached. Once we had aligned the corresponding intensity profiles, we calculated the efficiency of energy transfer $E = (I_{D,pb} - I_D)/I_{D,pb}$ across the wave, where I_D and $I_{D,pb}$, are the fluorescence intensities of the donor before and after bleaching, respectively (**Fig. 3b**, bottom). If MinE binds to MinD as a monomer and subsequently dimerizes to form the E-ring, the FRET efficiency would be low in the front and high in the rear of the wave. However, the FRET efficiency had a constant value of $E = 0.274 \pm 0.031$ (s.d., $n = 3$) (**Fig. 3b**, bottom) along the whole width of the wave. We also tested if the monomer-dimer equilibrium of MinE is affected by the presence of membrane-bound MinD. We found no change in either the FRET efficiency at equilibrium or the rate of FRET-efficiency increase during equilibration (**Supplementary Fig. 2**, **Supplementary Methods** and **Supplementary Discussion**). In conclusion, our FRET experiments show that MinE binds to MinD as a dimer and, consequently, MinE accumulation and E-ring formation do not reflect MinE dimerization.

Another explanation for the accumulation of MinE is cooperative binding: that is, the idea that MinE binding is enhanced by MinE already present in the wave band[13,18]. We sought to examine this possibility by adding fluorescent MinE (MinE-Cy5) to traveling waves of nonfluorescent MinE and MinD (doped with MinD–Alexa 488) and monitoring the incorporation of fluorescent MinE into the wave. If MinE from the solution bound preferentially to regions of high MinE densities, the intensity would increase faster at the rear of the wave than at the front. However, we observed that the initial maximum in MinE fluorescence was located close to the wave front, just in front of the maximum MinD–Alexa 488 intensity, in all experiments ($n = 4$, data from one experiment in **Fig. 3c**). Subsequently, the shape of the profile changed so that the fluorescence intensity increased faster at the trailing edge than at the leading edge, such that the MinE profile finally assumed the maximum at the trailing edge described above (**Fig. 3d**). We also conducted an analogous experiment in which we bleached Cy5-labeled MinE in the middle of the wave and then monitored fluorescence recovery during wave propagation (**Fig. 3e** and **Supplementary Fig. 3** and **Supplementary Discussion**). Even though the fluorescence at the rear of the wave was not decreased right after bleaching, it dropped while the wave was moving forward. This suggests that the bleached molecules, which were initially located in the front and middle of the protein band, accumulate at the rear during wave propagation.

Together, these results argue against cooperative attachment of MinE. Instead, they imply that MinE binding is dependent on the density of free MinD on the membrane, and that MinE then accumulates at the rear because of wave propagation.

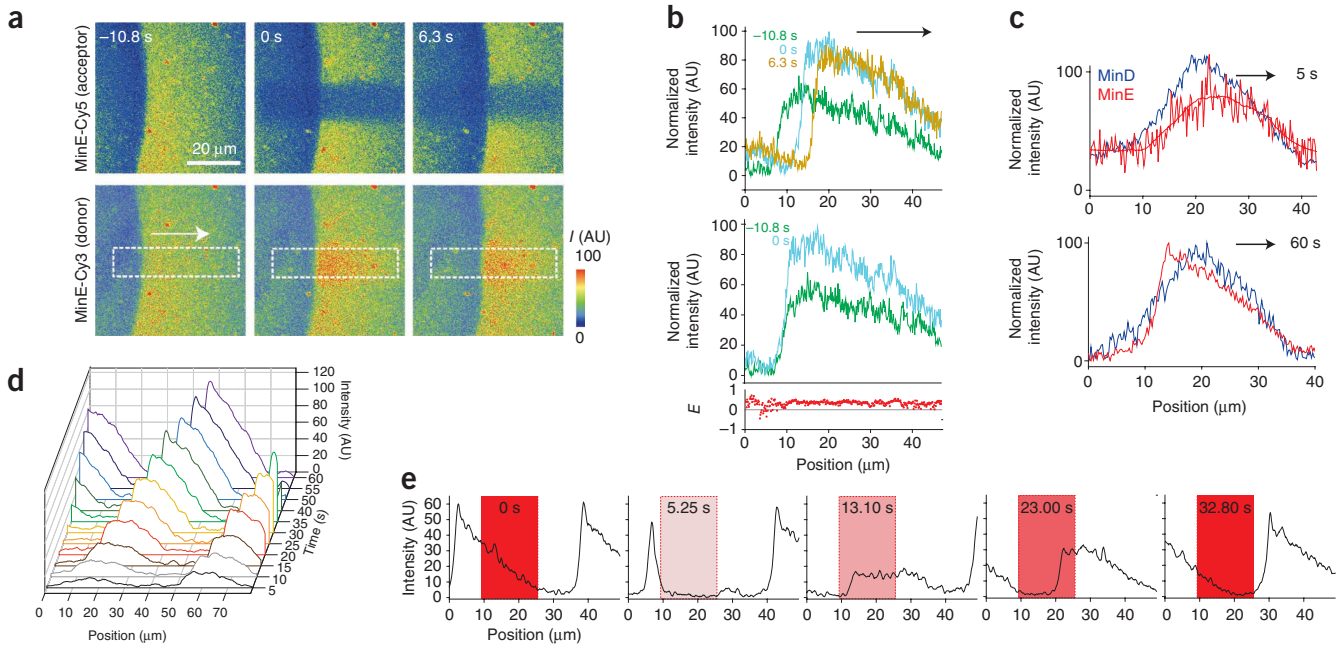

Figure 3 MinE accumulates at the rear of the wave during wave propagation. (**a**) FRET measurements by acceptor photobleaching. Confocal micrographs of MinD (0.65 μM), MinE-Cy5 (acceptor, 0.29 μM, final percentage of MinE-Cy5 = 40.0 mol %) and MinE-Cy3 (donor, 0.326 μM, final ratio of MinE-Cy3 = 40.6 mol %) before (at –10.8 s) and after bleaching of the acceptor (0 s and 6.3 s) (micrograph is pseudocolored to correspond to the fluorescence intensity). (**b**) Top, intensity profiles of the donor acquired from the rectangular areas shown in **a**. Bottom, aligned intensity profiles of the donor before and after bleaching (–10.8 s and 0 s). Below, calculated FRET efficiency along the width of the wave. (**c**) Intensity profiles for MinD (0.8 μM, doped with 10 mol % MinD–Alexa 488) and MinE (1.2 μM) shortly after addition of 0.015 μM MinE-Cy5 to traveling protein bands. Whereas in the initial profile (after 5 s), the maximum intensity of MinE-Cy5 is located in front of the MinD maximum, at steady state this maximum intensity is seen at the rear of the wave. (**d**) Intensity profiles corresponding to three traveling protein bands for ten successive frames after the addition of MinE-Cy5. (**e**) After bleaching MinE in the middle of the wave, the fluorescence intensity also drops in the rear while the wave is progressing forward. Only after the wave has left the previously bleached area is the fluorescence intensity fully recovered.

MinE accumulates by persistent binding

How does MinE pile up at the trailing edge of the moving protein 'carpet'? To study the behavior of individual Min proteins, we conducted single-molecule TIRF microscopy experiments. By decreasing the concentration of labeled protein to 10 nM, we could resolve single fluorescently labeled proteins on the membrane. Using Matlab-based single-particle tracking, we then analyzed the behavior of membrane-bound proteins.

We first measured the residence time and diffusion constant of MinD with no MinE present, when no waves were formed. We found that with increasing concentration of MinD, the mobility of the proteins was considerably reduced, from 0.425 ± 0.124 μm^2 s^{-1} at 0.275 μM to 0.013 ± 0.003 μm^2 s^{-1} at 1.1 μM (errors are ± s.d., $n = 4$; **Fig. 4a**,**b**). This low mobility at high densities argues for complete coverage of the membrane with MinD. Concurrently, the residence times of MinD increased from 11 s to 40.71 s. The later value is merely a lower limit of the residence times, because photobleaching occurred on a similar time scale. These findings suggest that at higher densities, intermolecular interactions become more likely, which allows MinD to bind more strongly to the membrane.

Next, we analyzed the behavior of single Min proteins in protein waves (**Fig. 4c**). While the waves were advancing, the proteins bound to the membrane, where they diffused and eventually detached (**Supplementary Videos 3** and **4**). We analyzed the attachment and detachment events of MinD, MinE and MinC in three different areas of the traveling protein band: in the leading 50% of the wave, in the middle and in the rear 20% of the wave (**Fig. 4d** and **Supplementary Figs. 4** and **5**). We found that for all proteins, binding dominates in the front and middle of the wave, whereas detachment dominates in the rear (**Fig. 4e** and **Supplementary Fig. 6**). This result further supports our arguments against cooperative MinE binding.

We then determined the diffusion constants of the proteins in the traveling wave. If the mobility of the proteins was the same everywhere in the wave, it would be described by a single Rayleigh distribution. However, we found large deviations from this distribution, which indicated varying mobilities (**Supplementary Fig. 5**). When we assigned the proteins to different parts of the wave as before, we obtained good fits for each of the different segments. Furthermore, we found that all three Min proteins slowed down considerably when they reached the wave's trailing edge (**Fig. 4f**, **Supplementary Fig. 6**). This is consistent with the observation that diffusivity decreases with increasing protein density in the absence of waves (**Fig. 4a**,**b**). This gradient of diffusivities suggests that MinD dimers bound to the membrane increasingly interact with each other, which leads to the formation of a focused, rather than blurred, protein band.

Next, we determined for how much time proteins remain bound to the membrane during wave propagation (**Fig. 4g**). Consistent with the extended residence times at higher protein densities in the homogenous state (**Fig. 4a**,**b**), we found that MinD, which detached from the rear of the wave, spent more time on the membrane than proteins, which detached from the middle or the front of the wave (8.72 ± 0.59 s, 6.53 ± 0.301 s and 4.57 ± 0.32 s, s.e.m, $n = 10$). The residence times of MinE, which did not bind to the membrane in the absence of MinD, also increased with increasing MinD density toward the rear of the wave, and, unexpectedly, were significantly longer than for MinD in every segment of the wave: 12.36 ± 1.05 s, 8.69 ± 0.84 s, 6.32 ± 0.78 s

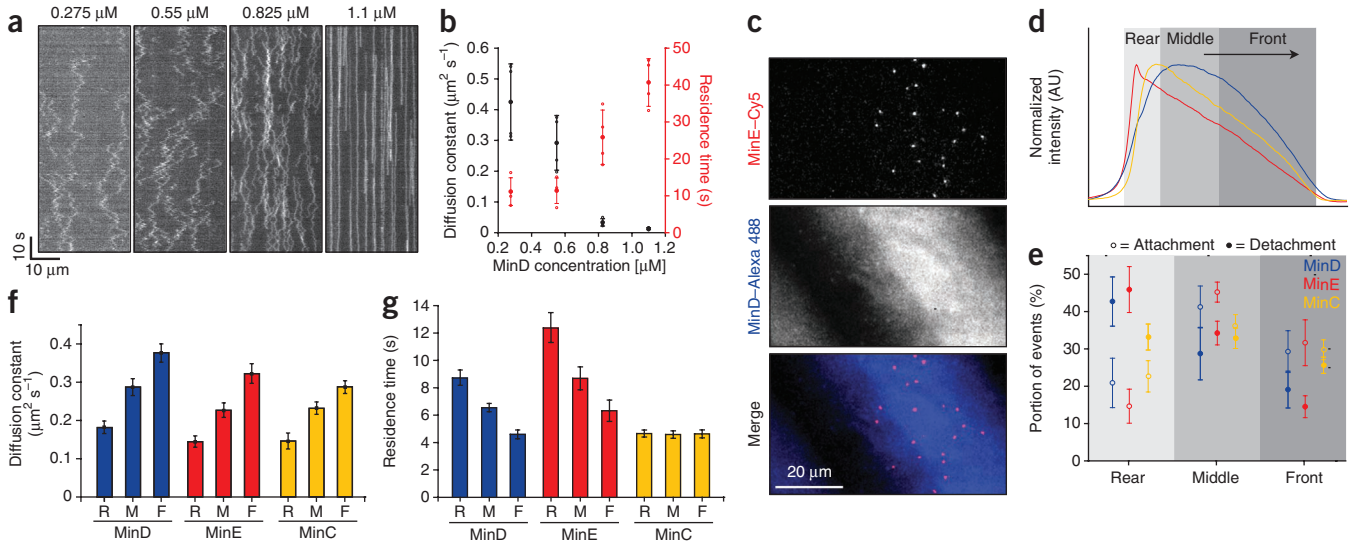

Figure 4 Single-molecule studies on Min proteins. (**a**) Behavior of single membrane-bound MinD dimers in the absence of waves. Kymographs along a 12-μm-thick line of membrane-bound Cy5-labeled MinD at different concentrations of nonlabeled MinD and without MinE. (**b**) Diffusion constants and residence times at different concentrations of MinD. With increasing protein concentration, membrane-bound MinD slows down while the average residence time increases. Error bars represent s.e.m. with $n = 4$. (**c**) Typical TIRF micrograph of single fluorescent Min proteins in traveling protein waves (MinE, 1.2 μM with 0.01 mol % MinE-Cy5; MinD, 0.8 μM with 5 mol % MinD–Alexa 488). (**d**) Normalized intensity profiles of Min proteins corresponding to **Figure 2**. The tracked particles were assigned to different segments of the wave, indicated in different shades of gray. (**e**) Portions of attachment and detachment events in different segments of the traveling protein band. (**f**) Diffusion constants of Min proteins in different segments of the traveling protein band. (**g**) Average residence times of Min proteins in different segments of the traveling protein band. The proteins were assigned to the different segments of the wave depending on where they detached from the membrane. R = rear, M = middle, F = front.

(s.e.m. $n = 10$, $P = 0.0032$, 0.0166, 0.0259). Although the observed difference between the residence times of MinE and MinD is small, it suggests that one MinE activates more than one MinD while it is part of the protein wave, a behavior we term 'persistent binding'. As a consequence, MinE can accumulate on the MinD carpet until all MinD dimers are in complex with MinE. In contrast to MinE and MinD, the residence times of eGFP-MinC were the same in every part of the wave and much shorter (4.66 ± 0.26 s, 4.56 ± 0.27 s, 4.63 ± 0.29 s), indicating a fast turnover of MinC (errors are ± s.e.m., $n = 10$ (MinD, MinE) or 7 (MinC)) (**Fig. 4g**).

Persistent binding implies that MinE should be able to diffuse on an immobile MinD carpet—in other words, on a saturated layer of membrane-bound MinD. Indeed, under these conditions, where no pattern was formed, we found MinE to have a three times higher diffusion constant than MinD (**Supplementary Fig. 7a**) but similar residence times (>30 s). This finding indicates that MinE is able to quickly change binding partners in a saturated layer of MinD without visibly detaching from the membrane.

Together, these results support the view that MinE accumulates toward the rear of the wave by persistent binding to a layer of membrane-bound MinD.

The role of MinE membrane interaction for pattern formation

Persistent binding of MinE could be realized either by transient membrane binding[22,27] or by fast rebinding before MinE is able to diffuse out of the interaction range with the membrane[20,21]. A recent study identified a mutant of MinE, termed MinE C1, which was shown to be fully capable of stimulating the MinD ATPase activity of MinD but to be deficient in membrane binding[27]. *In vivo*, the MinE C1 mutant was unable to support normal MinDE oscillation, implying that direct binding of MinE to the membrane plays a role during pattern formation of the Min system.

To investigate the role of membrane-binding for Min protein pattern formation, we tested MinE C1 in our *in vitro* assay. In agreement with the *in vivo* observations, we found that MinD and the MinE C1 mutant were unable to self-organize into a regular pattern of parallel surface waves. Instead, the pattern resembled a state transiently assumed by

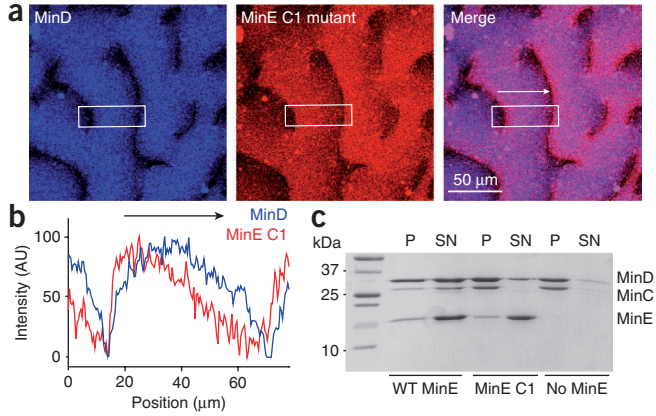

Figure 5 Membrane binding is not required for MinE accumulation. (**a**) Confocal fluorescence micrographs showing typical pattern formed by MinD and the membrane-binding deficient mutant MinE C1 (1.2 μM MinE C1 with 10 mol % MinE C1-Cy5 and 0.8 μM MinD with 10 mol % MinD–Alexa 488) on a supported lipid membrane. (**b**) Fluorescence intensity profiles of MinD and MinE C1 acquired from the rectangular region shown in **a**. Both proteins show a density distribution similar to those of the wild-type proteins. Toward the rear of the wave (left), the density of MinE C1 still rises when MinD is already detaching, as observed for WT MinE. However, MinE C1 does not form a peak at the rear of the wave. (**c**) In contrast to wild-type MinE, MinE C1 is not able to stimulate release of MinC and MinD from phospholipid vesicles.

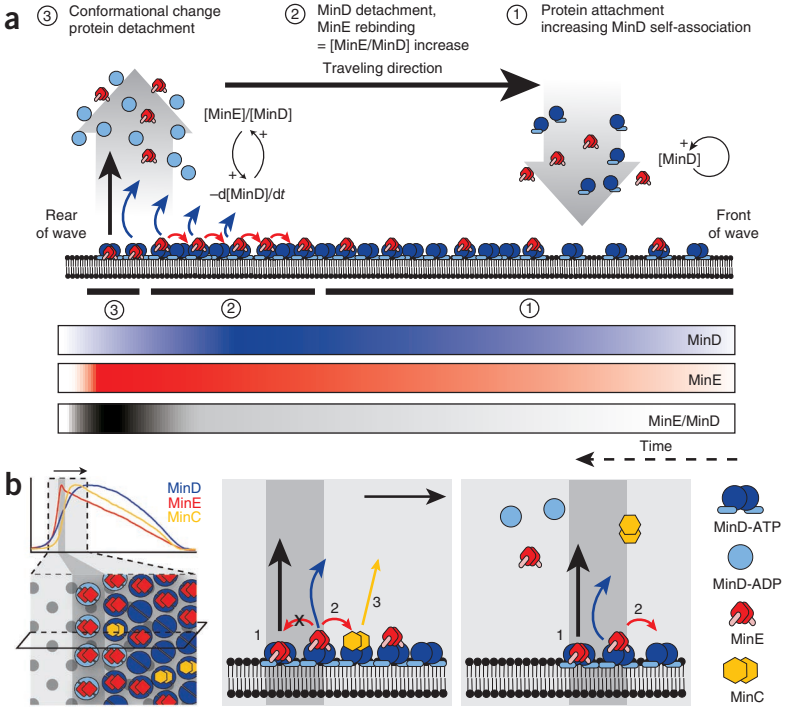

Figure 6 Model of Min-protein wave propagation. (**a**) Starting from the front of the protein wave (or at the beginning of an oscillation cycle, right), MinD-ATP starts to bind to the membrane. With increasing density, the MinD dimers bind longer to the membrane and diffuse more slowly (**Fig. 4**). MinE dimers bind to membrane-bound MinD, but the concentration of MinE is at first too low to result in membrane detachment becoming dominant. At a sufficiently high [MinE]/[MinD] ratio, protein detachment starts to dominate. Because of rapid MinE rebinding to MinD, the [MinE]/[MinD] ratio can continuously increase toward the rear of the wave. This behavior guarantees that eventually all membrane-bound MinD dimers are in complex with MinE. At a [MinE]/[MinD] ratio of about 1, interaction of MinE with the membrane induces a conformational change, which results in the displacement of all MinC (not shown here). Finally, all proteins rapidly leave the membrane. (**b**) Illustration of the order of events at the rear of the protein wave. Shown are top (left) and side (middle and right) views of Min proteins bound to the membrane. As seen in the side view, before detachment from the membrane, either MinE forms a complex with MinD, which is present in an altered conformation involving membrane binding by MinE (1), or MinE rebinds to a neighboring membrane-bound MinD, if available (2). Because the density of membrane-bound MinD is higher toward the front of the wave, rebinding MinE is biased in this direction, giving rise to the local saturation of MinD with MinE. After detachment of MinC from MinD (3), MinE can occupy the overlapping binding site on MinD.

wild-type proteins during synchronization toward parallel waves[13] (**Fig. 5a** and **Supplementary Video 5**).

Although the protein pattern was different, the fluorescence intensity distributions of MinD and MinE C1 in these ripples were similar to the distributions found in parallel waves formed by MinD and WT MinE; that is, the surface density of MinE C1 increased while MinD was detaching from the membrane (**Fig. 5a**,**b**). Similarly to the wild-type protein, the MinE C1 mutant diffused on an immobile layer of MinD (**Supplementary Fig. 7a**) and showed similar recovery behavior after photobleaching (**Supplementary Fig. 7b**), indicating that membrane binding is not required for MinE to interchange binding partners in the MinD layer bound to the membrane.

Remarkably, MinE C1 did not show a peak before detachment as WT MinE did (**Fig. 5b** and **Supplementary Fig. 7c**). Because this peak appeared to be involved in the exclusion of MinC from the MinD carpet, we were interested in the general ability of MinE C1 to displace MinC from MinD. After we added MinC to the traveling waves of MinE C1 and MinD, the protein waves disappeared and the proteins assembled into a homogeneous state, where only MinC and MinD were bound to the membrane, whereas MinE C1 was in solution. This finding was also confirmed in a sedimentation assay (**Fig. 5c**; see **Supplementary Methods**), where MinC co-sedimented with MinD and phospholipids despite the presence of MinE C1.

These data show that MinE C1 fails to displace MinC from MinD. One possible explanation for this could be that MinC displacement takes place because membrane binding by WT MinE leads to an allosteric transition that allows for a stronger interaction of MinE with MinD. We find it interesting that this interaction is apparently not required for the stimulation of MinD ATPase activity[27], MinE accumulation or the dynamic instability of the Min system. Nevertheless, membrane binding of MinE appears to contribute to the spatial and temporal robustness of pattern formation.

DISCUSSION

Based on our results, a picture for Min protein pattern formation emerges (**Fig. 6**). First, MinD binds cooperatively to the membrane and MinE dimers present in solution start to bind to membrane-bound MinD. Here, at the front of the wave, the [MinE]/[MinD] ratio is low, MinD can still accumulate on the membrane and binding of MinC to MinD is not yet affected by MinE. Toward the rear of the wave, however, the [MinE]/[MinD] density ratio continuously increases and detachment of MinD starts to dominate. The [MinE]/[MinD] ratio can further increase during MinD detachment, because rapid rebinding of MinE to membrane-bound MinD allows MinE to remain in the protein wave, occupying more and more MinD dimers still bound to the membrane. This behavior eventually gives rise to a zone of equimolar stoichiometry of MinE and MinD located at the rear of the wave. Here, the interaction of MinE with the membrane can induce a conformational change of the MinDE complex, giving rise to higher protein density. This structural change results in the displacement of MinC from the MinD carpet before the MinD–MinE complex itself detaches from the membrane. Furthermore, this interaction is able to increase the stability of Min-pattern formation, possibly by creating a diffusion barrier, which confines the protein band and enhances the directionality of the traveling wave.

We propose that the E-ring *in vivo* is formed by two complementary mechanisms: accumulation of MinE by rapid rebinding, and membrane interaction of MinE that induces a conformational change of the MinDE complex. Structural studies on the membrane-bound MinD–MinE complex could provide more information about how this is achieved on a molecular level.

What is the role of persistent binding of MinE in destabilizing the homogeneous distribution of Min proteins? As shown in **Figure 2**, the increase of the [MinE]/[MinD] ratio accelerates detachment of MinD.

Because MinE effectively remains bound to the MinD layer during MinD detachment, the [MinE]/[MinD] ratio rises further, additionally increasing the detachment rate of MinD. Accordingly, MinE would only detach when it cannot find an available MinD on the membrane. The overall result of these protein interactions is a positive feedback that accelerates protein detachment. A positive feedback is generally able to amplify small perturbations in a homogenous state[15,28] and can also explain how fluctuations in the [MinE]/[MinD] ratio can initiate symmetry breaking, starting from a homogenous protein distribution[13].

Theoretical studies have identified the cooperativity of MinD binding as a possible minimal requirement for dynamic instability in the Min system[29]. However, to capture the parallel protein waves observed *in vitro*, additional cooperative effects of MinE binding had to be included in the theoretical description[13]. The results of our study do not favor cooperativity of MinE binding; instead, the positive feedback we identified might be the missing component required to reproduce the observed *in vitro* patterns. Our mechanism for collective protein detachment needs to be tested by theoretical analysis.

To conclude, we believe that self-organization in the Min system arises from an interplay of two opposing mechanisms: cooperative binding of MinD to the membrane, and accelerated MinD detachment due to persistent MinE binding. The Min system fulfills the minimal requirements for proteins to switch collectively and repetitively between membrane-bound and cytoplasmic states[30–32]. Persistent binding of an activator to its nucleotide-hydrolyzing partner protein might represent a general motif for the collective detachment of proteins from intracellular membranes. This has also been proposed to be important for ParA-driven segregation of chromosomes in *Caulobacter crescentus*[32] and of low copy-number plasmids in *E. coli*[33].

METHODS

Methods and any associated references are available in the online version of the paper at http://www.nature.com/nsmb/.

Note: Supplementary information is available on the Nature Structural & Molecular Biology website.

ACKNOWLEDGMENTS

We would like to thank D. RayChaudhuri (Tufts University) for plasmid pZH101, J. Howard, S. Vogel and M. Mayer (all Max Planck Institute for Molecular Cell Biology and Genetics) for comments on the manuscript and D. Mullins (University of California, San Francisco) for discussions. M.L. received a scholarship from the Studienstiftung des deutschen Volkes. This work was also supported by the Max Planck Society (M.L., E.F.-F., P.S.).

AUTHOR CONTRIBUTIONS

M.L., P.S. and K.K. designed the research, M.L. conducted the research, E.F.-F. and C.H. wrote the tracking software, C.H. built the single-molecule TIRF setup, M.L. analyzed and interpreted the data with the help of all authors, and M.L., E.F.-F. and P.S. wrote the paper with the help of K.K.

COMPETING FINANCIAL INTERESTS

The authors declare no competing financial interests.

Published online at http://www.nature.com/nsmb/.
Reprints and permissions information is available online at http://www.nature.com/reprints/index.html.

1. Lutkenhaus, J. Assembly dynamics of the bacterial MinCDE System and spatial regulation of the Z ring. *Annu. Rev. Biochem.* **76**, 539–562 (2007).
2. Hu, Z., Mukherjee, A., Pichoff, S. & Lutkenhaus, J. The MinC component of the division site selection system in *Escherichia coli* interacts with FtsZ to prevent polymerization. *Proc. Natl. Acad. Sci. USA* **96**, 14819–14824 (1999).
3. Hu, Z. & Lutkenhaus, J. Topological regulation of cell division in *Escherichia coli* involves rapid pole to pole oscillation of the division inhibitor MinC under the control of MinD and MinE. *Mol. Microbiol.* **34**, 82–90 (1999).
4. Raskin, D.M. & de Boer, P.A. Rapid pole-to-pole oscillation of a protein required for directing division to the middle of *Escherichia coli*. *Proc. Natl. Acad. Sci. USA* **96**, 4971–4976 (1999).
5. Raskin, D.M. & de Boer, P.A. MinDE-dependent pole-to-pole oscillation of division inhibitor MinC in *Escherichia coli*. *J. Bacteriol.* **181**, 6419–6424 (1999).
6. Hale, C.A., Meinhardt, H. & de Boer, P.A. Dynamic localization cycle of the cell division regulator MinE in *Escherichia coli*. *EMBO J.* **20**, 1563–1572 (2001).
7. Hu, Z. & Lutkenhaus, J. Topological regulation of cell division in *E. coli*. spatiotemporal oscillation of MinD requires stimulation of its ATPase by MinE and phospholipid. *Mol. Cell* **7**, 1337–1343 (2001).
8. Hu, Z. & Lutkenhaus, J. Analysis of MinC reveals two independent domains involved in interaction with MinD and FtsZ. *J. Bacteriol.* **182**, 3965–3971 (2000).
9. de Boer, P.A., Crossley, R.E. & Rothfield, L.I. Central role for the *Escherichia coli* minC gene product in two different cell division-inhibition systems. *Proc. Natl. Acad. Sci. USA* **87**, 1129–1133 (1990).
10. de Boer, P.A., Crossley, R.E. & Rothfield, L.I. Roles of MinC and MinD in the site-specific septation block mediated by the MinCDE system of *Escherichia coli*. *J. Bacteriol.* **174**, 63–70 (1992).
11. Lackner, L.L., Raskin, D.M. & Boer, P.A.J.d. ATP-dependent interactions between *Escherichia coli* Min proteins and the phospholipid membrane *in vitro*. *J. Bacteriol.* **185**, 735–749 (2003).
12. Hu, Z., Saez, C. & Lutkenhaus, J. Recruitment of MinC, an inhibitor of Z-ring formation, to the membrane in *Escherichia coli*: role of MinD and MinE. *J. Bacteriol.* **185**, 196–203 (2003).
13. Loose, M., Fischer-Friedrich, E., Ries, J., Kruse, K. & Schwille, P. Spatial regulators for bacterial cell division self-organize into surface waves *in vitro*. *Science* **320**, 789–792 (2008).
14. Kruse, K. & Jülicher, F. Oscillations in cell biology. *Curr. Opin. Cell Biol.* **17**, 20–26 (2005).
15. Novák, B. & Tyson, J.J. Design principles of biochemical oscillators. *Nat. Rev. Mol. Cell Biol.* **9**, 981–991 (2008).
16. Mileykovskaya, E. *et al.* Effects of phospholipid composition on MinD-membrane interactions *in vitro* and *in vivo*. *J. Biol. Chem.* **278**, 22193–22198 (2003).
17. Lackner, L.L. *Investigating the Mechanism of Escherichia coli Min Proteins Dynamics*. PhD thesis, Case Western Reserve Univ. (2006).
18. Meinhardt, H. & de Boer, P.A. Pattern formation in *Escherichia coli*: a model for the pole-to-pole oscillations of Min proteins and the localization of the division site. *Proc. Natl. Acad. Sci. USA* **98**, 14202–14207 (2001).
19. Huang, K.C., Meir, Y. & Wingreen, N.S. Dynamic structures in *Escherichia coli*: spontaneous formation of MinE rings and MinD polar zones. *Proc. Natl. Acad. Sci. USA* **100**, 12724–12728 (2003).
20. Meacci, G. & Kruse, K. Min-oscillations in *Escherichia coli* induced by interactions of membrane-bound proteins. *Phys. Biol.* **2**, 89–97 (2005).
21. Derr, J., Hopper, J.T., Sain, A. & Rutenberg, A.D. Self-organization of the MinE protein ring in subcellular Min oscillations. *Phys. Rev. E* **80**, 011922 (2009).
22. Arjunan, S.N.V. & Tomita, M. A new multicompartmental reaction-diffusion modeling method links transient membrane attachment of *E. coli* MinE to E-ring formation. *Syst. Synth. Biol.* **4**, 35–53 (2010).
23. Szeto, T.H., Rowland, S.L. & King, G.F. The dimerization function of MinC resides in a structurally autonomous C-terminal domain. *J. Bacteriol.* **183**, 6684–6687 (2001).
24. de Boer, P.A., Crossley, R.E., Hand, A.R. & Rothfield, L.I. The MinD protein is a membrane ATPase required for the correct placement of the *Escherichia coli* division site. *EMBO J.* **10**, 4371–4380 (1991).
25. Galush, W.J., Nye, J.A. & Groves, J.T. Quantitative fluorescence microscopy using supported lipid bilayer standards. *Biophys. J.* **95**, 2512–2519 (2008).
26. Verveer, P.J., Rocks, O., Harpur, A.G., Bastiaens, P.I.H. Measuring FRET by acceptor photobleaching. in *Protein-Protein Interactions: A Molecular Cloning Manual*, Vol. 2 (eds. Golemis, E. & Adams, P.D.) 4598–4601 (Cold Spring Harbor Press, Cold Spring Harbor, NY, USA, 2005).
27. Hsieh, C.-W. *et al.* Direct MinE-membrane interaction contributes to the proper localization of MinDE in *E. coli*. *Mol. Microbiol.* **75**, 499–512 (2010).
28. Ferrell, J.E. & Xiong, W. Bistability in cell signaling: how to make continuous processes discontinuous, and reversible processes irreversible. *Chaos* **11**, 227–236 (2001).
29. Kruse, K., Howard, M. & Margolin, W. An experimentalist's guide to computational modelling of the Min system. *Mol. Microbiol.* **63**, 1279–1284 (2007).
30. Tyson, J.J., Chen, K.C. & Novak, B. Sniffers, buzzers, toggles and blinkers: dynamics of regulatory and signaling pathways in the cell. *Curr. Opin. Cell Biol.* **15**, 221–231 (2003).
31. Howard, J. & Hyman, A.A. Growth, fluctuation and switching at microtubule plus ends. *Nat Rev. Mol. Cell. Biol.* **10**, 569–574 (2009).
32. Ptacin, J.L. *et al.* A spindle-like apparatus guides bacterial chromosome segregation. *Nat. Cell Biol.* **12**, 791–798 (2010).
33. Ringgaard, S., van Zon, J., Howard, M. & Gerdes, K. Movement and equipositioning of plasmids by ParA filament disassembly. *Proc. Natl. Acad. Sci. USA* **106**, 19369–19374 (2009).

ONLINE METHODS

Protein expression and purification. His-MinD and His-MinE were purified and fluorescently labeled[13]. To obtain pET28a-His-MinC, pZH101 (see ref. 2) (D. RayChaudhuri) was digested with EcoRI and SalI, and the MinC fragment was ligated into pET28a treated with EcoRI and XhoI. The resulting reading frame encoded for MinC connected to an N-terminal hexahistidine tag by a linker, a thrombin cleavage site and a T7 tag . To obtain pET28a-His-eGFP–MinC, a PCR fragment containing an N-terminal hexahistidine tag and the gene that encodes eGFP was amplified from pEGFP-N2 using the primers 5′-GGC CTG TCA TGA GAC ATC ATC ATC ATC ATC ACG TGA GCA AGG GCG AGG AGC-3′ and 5′-GCG TGA ATT CAC CCG CTG CAC CCT TGT ACA GCT CGT CCA TGC CG-3′. This fragment was treated with BspHI and EcoRI and ligated into pET28a-His-MinC that was digested with NcoI and EcoRI. The resulting ORF was encoded for fusion protein of eGFP–MinC with an N-terminal hexahistidine tag. His-MinC was expressed and purified as His-MinD and His-MinE. For His-eGFP–MinC expression, cells were induced with 1 mM IPTG at an optical density of 0.8 and grown overnight at 16 °C.

Self-organization assay. Self-organization experiments of Min proteins were conducted as previously described[13]. For studies on MinC, MinC was doped with 30 mol % His-eGFP–MinC. For TIRF microscopy experiments, glass cover slips were rinsed with alcohol and cleaned in air plasma. The mica sheet was attached with immersion oil such that the exciting beam was reflected at the mica-water interface. A plastic ring was glued with ultraviolet-resistant glue directly onto the mica to form the incubation chamber. To observe single molecules, 0.01 mol % of labeled molecules were added (MinD or MinE labeled with Cy5 or eGFP-MinC). A high proportion of variously labeled molecules was added (in the case of Cy5-labeled proteins, MinE or MinD was labeled with Alexa 488 and, in the case of eGFP-MinC, MinE or MinD was labeled with Cy5) to monitor wave propagation. Residence times of the proteins were assigned to a specific zone in the wave band according to where the protein detached from the membrane.

Diffusion constants and residence times of MinE and MinD were determined in the absence of MinC. Total protein concentrations for the single molecule experiments were MinD, 0.8 μM; MinE, 1.2 μM; and MinC, 0.05 μM. Photobleaching of the dye was reduced by adding an oxygen scavenger system (glucose oxidase (165 U ml^{-1}) catalase (2,170 U ml^{-1}), β-D-glucose (0.4% w/v) and Trolox (2 mM), all from Sigma). In the case of eGFP-MinC, 1 mM DTT was used instead of Trolox.

Imaging. Confocal imaging was conducted using a Zeiss LSM 510 microscope with a Zeiss C-Apochromat 40×, numerical aperture (NA) = 1.2, water-immersion objective, at 20 °C. The fluorescence signal was detected with a photomultiplier. TIRF microscopy experiments were carried out on a setup built around an Axiovert 200 microscope (Zeiss). The 488-nm and 647-nm lines of an Innova70-Spectrum Argon/Krypton laser (Coherent), selected using an acousto-optical tunable filter (AA Opto-Electronic), were used to excite fluorescently labeled proteins. Before entering the microscope, the laser beam passed through a combination of a polarizer and a λ/4-plate, and was focused at the back focal plane of a Zeiss α 'Plan-Fluar' 100× /1.45 oil immersion or α Plan-Apochromat 100× /NA 1.46 oil immersion objective. Fluorescence light was separated from the laser lines using a FF497/661 dichroic filter (Semrock) and was split into two spectral channels using a W-View beam splitter (Hamamatsu), and directed to an Andor iXon EM-CCD camera. The camera resolution was 156 nm per pixel. Videos were recorded using a frame rate of 5 frames s^{-1} and an exposure time of 50 ms. Fluorescence intensity profiles were obtained using ImageJ (W.S. Rasband). Smoothing of intensity profiles was conducted using the Savitzky-Golay method implemented in Origin (OriginLab).

Single-molecule analysis. Videos of single Min proteins were analyzed using image analysis software written in Matlab, based on the IDL Particle Tracking software[34] .

The Matlab routines for finding and tracking particles were developed by D. Blair and E. Dufresne (http://www.physics.georgetown.edu/matlab/). Raw images were background corrected with a boxcar average and convolved with a Gaussian kernel to suppress high-frequency noise. The program first identifies peaks in the pixel intensity values above a threshold brightness for a single frame of the video. Intensity peaks are assigned (x,y) position values by finding local intensity maxima in an image-to-pixel level accuracy. By fitting the intensity around each particle to a two-dimensional Gaussian curve, the position is determined to subpixel accuracy. For each intensity peak, the program calculates the position (x_i,y_i), the brightness and the square of the radius of gyration. Next, the program examines subsequent video frames and constructs trajectories from a list of particle coordinates determined at discrete times by a global minimization of the sum of the square of particle displacements between frames[34]. The maximal displacement between two successive frames was set to 9 pixels, which corresponds to 1.422 μm. The program occasionally lost particles during tracking. To compensate for this error, we allowed particles to disappear for two frames while they were bound to the membrane. The minimum track length was four frames. To exclude stationary particles, those which were nonspecifically bound to the membrane, the average displacement of a particle during its entire stay on the membrane was required to be larger than 0.8 pixels, which is equal to 0.1248 μm. The remaining tracks comprise the dataset (x,y positions for each particle, and the corresponding frame number) for further analysis using a custom-written Matlab code. One independent experiment represents one individual self-organized pattern formed on an individual supported membrane. During each experiment, 5–15 videos were acquired. For each video (between 500 and 700 frames with a total run length of 100–140 s), a minimum number of 100 protein tracks were analyzed. Therefore, one experimental value represents the average of at least 500 analyzed tracks for each of the three Min proteins. The averaged value of ten experiments represents at least 5,000 analyzed tracks.

34. Crocker, J. & Grier, D. Methods of digital video microscopy for colloidal studies. *J. Colloid Interface Sci.* **179**, 298–310 (1996).

doi:10.1038/nsmb.2037